Workflow for upscaling wettability from the nano- to core-scales

Maja Rücker[1,3], *Willem-Bart* Bartels[2,3], *Tom* Bultreys[1,4,6], *Marijn* Boone[7], *Kamaljit* Singh [5,6], *Gaetano* Garfi [6], *Alessio* Scanziani [6], *Catherine* Spurin[6], *Sherifat* Yesufu [1], *Samuel*. Krevor[6], *Martin. J.* Blunt[6], *Ove* Wilson[3], *Hassan* Mahani[3], *Veerle* Cnudde[2,4], *Paul F.* Luckham[1], *Apostolos* Georgiadis[1,3] and *Steffen* Berg[1,3,6]

[1]Department of Chemical Engineering, Imperial College London, UK
[2]Earth Sciences Department, Utrecht University, NL
[3]Shell Global Solutions International B.V., Grasweg 31, 1031 HW Amsterdam, NL
[4]UGCT- PProGRess, Ghent University, BE
[5]Institute of Petroleum Engineering, Heriot-Watt University, Edinburgh, UK
[6]Department of Earth Science and Engineering, Imperial College London, UK
[7]Tescan XRE, Bollenbergen 2B bus 1, 9052 Ghent, BE

Abstract. Wettability is a key factor influencing multiphase flow in porous media. In addition to the average contact angle, the spatial distribution of contact angles along the porous medium is important, as it directly controls the connectivity of wetting and non-wetting phases. The controlling factors may not only relate to the surface chemistry of minerals but also to their texture, which implies that a length-scale range from nanometres to centimetres has to be considered. So far, an integrated workflow addressing wettability consistently through the different scales does not exist. In this study, we demonstrate that such a workflow is possible by combining micro-computed tomography imaging with atomic force microscopy (AFM). We find that in a carbonate rock, consisting of 99.9% calcite with a dual porosity structure, wettability is ultimately controlled by the surface texture of the mineral. Roughness and texture variation within the rock control the capillary pressure required for initializing proper crude-oil-rock contacts that allow ageing and subsequent wettability alteration. AFM enables us to characterize such surface-fluid interactions and to investigate the surface texture. In this study, we use AFM to image nano-scale fluid-configurations *in situ* in 3D at connate water saturation and compare the fluid configuration with simulations on the rock surface assuming different capillary pressures.

1 Introduction

Wettability is the preference of a solid to be in contact with one fluid over another fluid. In petroleum applications, rock represents the solid phase, crude oil the first fluid phase and brine, which may be either present in the reservoir (formation water) or injected for oil recovery, the second fluid phase. A rock surface is called water-wet when the water tends to cover it and is called oil-wet when it prefers to be in contact with the oil phase. Furthermore, wettability may vary from location to location with a mixture of water-wet and oil-wet regions. In this case the rock is called mixed-wet [1-5].

Wettability by itself is not a property used as a direct input parameter for reservoir models. Yet, it is known to significantly impact input values such as relative permeability- and capillary pressure-saturation functions [6-8]. So far, these relationships can only be determined with core-scale experiments. To predict these parameters for a specific reservoir a better understanding of the principles behind wettability is crucial.

In a reservoir the wettability depends on various properties which act at different length scales. An overview of the different properties over increasing length scales is shown in Fig. 1. Brine and crude oil composition, surface chemistry and the P-T conditions affect molecular interactions, which can be assessed for instance through adhesion force measurements obtained with atomic force microscopy (AFM) [9-11].

At the sub pore scale, roughness, which may facilitate formation of thin water- or oil-films, becomes an additional factor. On this length scale the contact angle forming along three-phase contact lines may be measured [12].

At the larger pore and pore-network scale (μm to mm), the confined space within a porous medium is taken into account. Mineralogy and mineral distribution as well as the saturation history need to be considered. On this length scale wettability can be characterized through contact angle distributions [13], fluid distributions [14], by defining local capillary pressure [15, 16] and small scale relative permeability [17, 18].

To predict wettability at the core scale the contribution of each consecutive scale to the overall wettability of the system needs to be considered.

* Corresponding author: m.rucker15@imperial.ac.uk

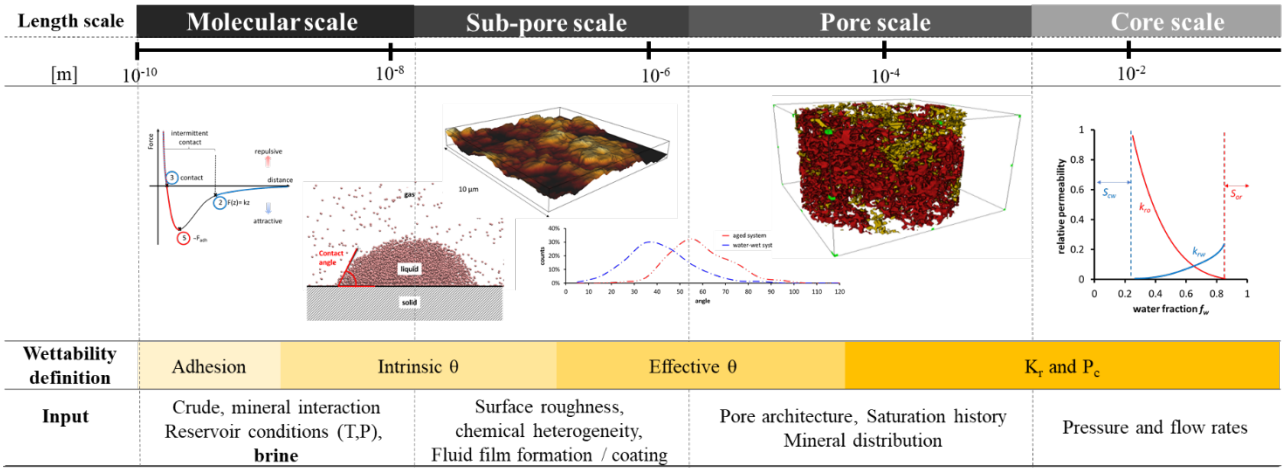

Fig. 1. Wettability depends on various properties acting at different length scales such as brine- and crude-oil composition, reservoir pressure and temperature (P-T) conditions, surface chemistry associated with mineralogy at the molecular scale, surface structure and fluid-film formation at the sub-pore scale as well as saturation history and mineral distribution at the pore scale. They all influence wettability, and thereby the pore-dynamics during two-phase flow and the relative permeability. [71]

1.1 Wettability at the molecular scale

Most minerals of reservoir rock are originally strongly water-wet [4, 9, 19]. However, the adsorption of surface active components or the precipitation of asphaltenes present in the crude oil may alter the wettability towards more oil-wet [4, 20-23]. Correspondingly, crude oils are usually classified by assessing their acid (TAN) and base (TBN) numbers as well as saturate, aromatics, resins and asphaltene (SARA) fractions, which indicate the stability of asphaltenes within the crude [24, 25].

In addition to the chemistry of the crude oil and the rock, the brine composition may also impact the wettability. Along a mineral surface, the balance between electro-static forces and van der Waals forces leads to a double layer of counter ions of the brine phase in correspondence with Derjaguin-Landau-Verwey-Overbeek [26, 27] (DLVO theory), which impacts the repulsive/attractive forces of approaching oil molecules [28, 29].

Various studies addressed the impact of these different components [30-33]. In this work, we keep these values constant by focussing on specific crude oil/rock/brine systems to assess the impact of various parameters controlling wettability at larger length scales.

1.2 Wettability at the sub-pore scale

At the sub-pore scale the measure of wettability is the contact angle, which can be obtained by imaging a droplet on a surface e.g. with a contact angle goniometer [34-41]. However, sub-resolution features are known to impact the observed response. Surface roughness may lead to pinning and therewith to a range of possible equilibrium contact angles [12, 42, 43]. This effect even occurs on surfaces considered atomically flat [42, 44]. Correspondingly, any contact angle measured represents an effective contact angle θ_e. The intrinsic contact angle θ_i, which is solely related to the molecular interactions, is only a theoretical descriptor obtained e.g. through

Table 1. TAN, TBN, SARA fractions, viscosity and density of the crude oils used.

	TAN [mg KOH g^{-1}]	TBN [mg kg^{-1}]	Saturates [wt %]	Aromatics [wt %]	Resins [wt %]	Asphaltenes [wt %]	Viscosity 20 °C [mPa s]	Density 20 °C [g cm^{-3}]
crude A	0.07	83.9	58.45	44.00	4.36	0.28	4.87	0.83
crude B	0.38	2.86	52.08	39.06	7.96	0.91	17.03	0.85

Table 2. Composition of formation water (FW) and a high salinity brine (HS) used.

ION [mg/L]	Na^+	K^+	Mg^{2+}	Ca^{2+}	Cl^-	SO_4^{2-}	HCO^{3-}	I^-	Ionic strength [mol/L]	pH
FW	49898	0	3248	14501	111812	234	162	0	3.659	6.9
HS (doped)	0	47106	0	0	0	0	0	152894	1.205	-
S (doped)	0	21198	0	0	0	0	0	68802	0.542	-

molecular models assuming a perfectly smooth surface with the fluid phases being equilibrated [12, 45].

Dynamic contact angle measurements allow the assessment of roughness through an advancing contact angle θ_a and receding contact angle θ_r, which represent the upper and lower boundary of possible contact angles for the studied surface. The detected contact angle hysteresis depends on the intrinsic contact angle, the surface roughness and velocity of the moving contact line [12].

Furthermore, grooves on a rough surface lead to entrapment of the wetting phase [46-48]. This can have large effects on the wettability alteration process. During drainage, in most cases the aqueous phase is wetting and forms water-films and layers within such grooves. These water-films and layers prevent the intimate contact between the oil and the solid and therewith wettability alteration in this regions Correspondingly, such water films may lead to mixed wettability patterns along the surface [3, 22, 49, 50].

1.3 Wettability at the pore scale

So far, most 3D studies on mixed-wet and oil-wet rock systems have focussed on wettability characterization. Andrew et al. [13] introduced *in situ* measurements of contact angles in rock and Scanziani et al. [51] and AlRatrout et al. [52] automated the process. Contact angle distributions are sensitive to image resolution and may vary in case of non-equilibrium conditions [13]. However, they provide an indication of the wettability and wettability changes of the system. Alhammadi et al. [53] showed a shift of the contact angle distribution when the wettability of the rock is altered by aging. Yet, these contact angles are not sufficient for prediction of larger scale relative permeabilities. The obtained distribution does not necessarily cover the advancing contact angle θ_a, which is used as input for most multiphase flow models in porous media, nor for its spatial distribution in case of a mixed-wet rock [17].

Another way to characterize wettability is through fluid distribution. In oil-wet and mixed-wet systems the oil clusters appear sheet-like and flat compared to the more spherical geometry in water-wet systems [54, 55]. Singh et al. [56] observed oil layer formation on the rock surface and between two water interfaces, which provides a conductive flow path for the oil phase in mixed-wet systems. Lin et al. [57] observed the formation of minimal fluid-fluid interfaces with a mean curvature of approximately zero and deviating principal curvatures. The fluid phase distribution or geometry may be fully characterized through morphological descriptors known as the four Minkowski functionals: volume, surface area, integrated mean curvature and Euler characteristic [14, 58-62].

Recent work focuses on linking the pore scale wettability parameter to core scale properties such as capillary pressure -saturation and relative permeability - saturation relationships [16, 18, 63-65].

1.4 Wettability at the core scale

In conventional special core analysis (SCAL) experiments, the capillary pressure - saturation relationship is used to assess the wettability of a system. This relationship can be obtained by combining the Amott spontaneous imbibition test, in which the cumulative production of the displaced phase versus time is recorded as well as waterfloods to obtain the forced part of the capillary pressure. Various indices, with the Amott and USBM index being the most common, have been introduced to derive wettability from the capillary pressure - saturation relationship [66, 67]. However, the results of such experiments are difficult to interpret as other factors besides wettability may impact the results. These factors include, for instance, viscosity, interfacial tension and flow dynamics [68-70]. An alternative is the wettability characterization by re-scaling the Leverett J function to provide an average contact angle [71, 72]. Yet, this method is not able to account for mixed wettability.

The wettability of a system can also be inferred from the relative permeability- saturation functions using the end-point water relative permeability, oil-layer drainage and shape of the water relative permeability: An end point permeability $\boldsymbol{k_{rw}^{max}} < 0.3$ indicates a water-wet system, $0.3 < \boldsymbol{k_{rw}^{max}} < 0.6$ a mixed wet and $\boldsymbol{k_{rw}^{max}} > 0.6$ an oil-wet system. Oil-layer drainage can be assessed from k_{ro} near to the end-point: If $k_{ro} < 0.05$, while the saturation is still decreasing, oil is moving through a continuous oil layer, which is indicative of a mixed- or oil-wet system. If the shape of k_{rw} shows a sharp rise with a cross over saturation $\boldsymbol{S_w^{cross}} < 0.5$ the system is often oil-wet. A low $k_{rw} < 0.2$ for $S_w = S_{wi} + 0.2$ is indicative of a water-wet system [73].

To predict the described core-scale output using computational models this behaviour needs to be linked to the smaller scale wettability responses. In this work we combine the results of various experiments across length scales using similar systems to describe this relationship.

2 Methodology

In this work, we compiled the results of previous studies addressing wettability in similar systems [49, 74-77] and complemented the results with additional measurements to obtain wettability descriptions across all length scales.

2.1 Sample selection

1.1.1 Crude oil

The crude oils were chosen based on their high wettability alteration potential. The corresponding total acid number (TAN) and total base number (TBN) as well as the Saturates, Aromatics, Resins, Asphaltene (SARA) analysis are listed in Table 1. The crude oils are rich on surface active components and asphaltenes, which represent the components that are expected to change the wettability of the rock.

Crude oil B was doped with 20% - iododecane, to enhance the contrast to the brine phase for µCT imaging.

In all experiments with crude oil A, the brine phase was doped with potassium iodide. In one experiment, n-decane was used as a model oil.

1.1.2 Brine

The brine composition used in the current studies is listed in Table 2. The formation water (FW) recipe, typical for a carbonate reservoir, was taken from Mahani et al. [78]. For the first study with a doped brine a 17 wt% KI-brine was chosen. Based on the ionic strength this corresponds to 70400 ppm NaCl and therefore is considered a high salinity solution (HS). For the other experiment a 9 wt% KI-brine (S) was chosen to obtain better contrast between the two fluid phases.

1.1.3 Rock

Ketton rock is a middle Jurassic oolithic carbonate rock consisting of round grains (ooids and peloids) ranging from 100 µm – 1 mm size. Oolites are marine sediments, which form during evaporation. Dissolved carbonate precipitates along nuclei floating in the seawater, which leads to concentric growth and to the round shape of the grains. Once the particles become too heavy they accumulate at the seafloor, where they become cemented [79]. The geological history of the formation leads to a homogeneous and simple structure of the rock, which makes the rock highly suitable for µCT flow experiments [49, 80, 81].

The rock has a porosity of φ = 23% with a bimodal pore size distribution and permeability of 3 – 6 D. It consists predominantly of calcite (99.1%) with minor quartz (0.9%) components [82].

2.2 Core scale wettability assessment

At the core scale, wettability can be derived from relative permeability-saturation and capillary pressure-saturation functions. These can be obtained through special core analysis (SCAL) experiments such as steady-state core floods or Amott spontaneous imbibition tests.

2.2.1 Steady-state core flood experiment

Experiments to determine relative permeability were performed in a custom-built X-ray saturation measurement apparatus at Shell [18, 83, 84] following the steady-state method [85, 86].

The Ketton sample (SCAL-plug: diameter d = 2.5 cm and length L = 5 cm) was first saturated with HS-brine and then mounted inside an X-ray transparent core holder and placed in the flow apparatus for steady-state relative permeability measurement. Afterwards, the sample was desaturated with crude oil A by flooding at 1 ml/min until no further change in saturation was detected. The sample was then aged at 30 bar and 70˚ C for 1 week. The measurements were conducted at a constant flow rate, where the fractional flow f_w was systematically changed from 100% crude oil to 100% brine in 10 steps (f_{w1} = 0,01; f_{w2} = 0,05; f_{w3} = 0,1; f_{w4} = 0,3; f_{w5} = 0,5; f_{w6} = 0,7; f_{w7} = 0,9; f_{w8} = 0,95; f_{w1} = 0,99; f_{w10} = 1). At each step saturation (and spatial profile along the core) and phase pressures were recorded after steady-state was reached. The SCAL data (pressure drop over the core and *in situ* saturation profiles at each fractional flow step) were matched numerically using Shell's in-house simulator (MoReS) to estimate the relative permeability as a function of saturation.

2.2.2 Amott spontaneous imbibition tests

In an Amott spontaneous imbibition test an oil-saturated rock sample is placed into a vessel containing brine. In water-wet and mixed-wet samples the water starts to spontaneously imbibe into the rock sample replacing the oil, which then gets produced, collected and monitored over time. The production rate and the cumulative production are used as a measure for wettability [67].

Bartels et al. [77] conducted an Amott spontaneous imbibition test on a SCAL plug sample and a mini plug sample commonly used for µCT studies (mini-plug: diameter d = 4 mm and length L = 20 mm).

Both samples were cleaned, saturated with brine and then desaturated with crude oil B. The SCAL plug was desaturated by centrifugation (URC-628, 129 Coretest Systems Inc., used at 3500 RPM) for 24 hours while the temperature was kept constant at 40˚C. The mini plug was desaturated by flooding 0.5 ml/min and then placed into an oven at 40 ˚C for 24 h.

Consecutively the samples were placed into Amott vessels. The production of the SCAL plug was monitored with HECTOR, a high energy µCT scanner at the Centre for X-ray Tomography (UGCT) in Ghent, Belgium [87] and the production of the mini plug with the Environmental MicroCT scanner (EMCT) also at UGCT [88]. The scans were reconstructed using dedicated reconstruction tools in the Acquila software package from Tescan XRE. Visualization and additional post-processing of the data were performed with Avizo 9.2.0 (Thermo Fischer Scientific).

The detailed experimental procedures can be found in Bartels et al. [77].

2.3 Pore scale wettability assessment

Lin et al. [89] stated that sample initialization, especially flooding as opposed to centrifugation may have a significant impact on the outcome. For this reason, both initialization protocols (centrifugation and flooding) were assessed at the pore scale.

2.3.1 Unsteady-state waterflood experiments initialized by flooding

The unsteady-state waterflood experiment was obtained from Rücker et al, [90]. The mini plug samples were first saturated with HS brine and then desaturated with crude A by flooding 0.5 ml/min using the flow cell described in Armstrong et al. [13]. The samples were aged at 3MPa

and 70 ˚C for one week. The waterflood was performed at a flow rate of 0.03 ml/min. During the experiment the fluid distributions within the sample were monitored using fast µCT facility at the TOMCAT-SLS beamline at the Paul Scherrer Institute, PSI, in Switzerland, while the HS brine was injected into the sample.

The images were reconstructed using the Paganin method [91] and processed and segmented with Avizo 9.0. The wettability of the system was assessed visually and by contact angle measurements following the workflow described in Andrew et al. [13] using the filtered grey scale image of the final timestep measured during this flooding sequence.

2.3.1 Unsteady-state waterflood experiments initialized by centrifugation

The unsteady-state waterflood performed on a centrifuged sample was prepared following the protocols from Lin et al. [89]. 8 subsamples with a diameter ø = 6 mm and length L = 20 mm were predrilled in a SCAL plug with a diameter ø = 3.8 cm and length *L* = 4 cm. Subsequently, the plug was saturated with HS-brine, desaturated in a centrifuge with crude A (URC-628, 129 Coretest Systems Inc., used at 3500 RPM for 24h) and then stored under elevated pressure of 3 MPa and temperature of 70 °C for 4 weeks. Afterwards, the smaller sample was chopped off the SCAL plug and fitted into the Viton sleeve while being kept in the crude oil and placed into a core holder described in Singh et al. [56]. Consecutively, a waterflood experiment was performed by injecting HS-brine at a flow rate of 0.03 ml/min for 2 h. µCT scans with a voxel size of 6.1 µm were taken for the full sample and two smaller (988 ×1014 × 997) subsamples with a voxel size of 2 µm prior to and after the experiment using a Xradia µCT-scanner (Zeiss).

The images were reconstructed using the proprietary software provided by Zeiss, filtered with a non-local means filter and segmented with the trainable WEKA segmentation tool [92] provided by Fiji [93]. The contact angle distribution was measured manually using the filtered image obtained after the waterflood following the procedure described in Andrew et al. [13]

2.3 Topographical measurements with AFM

At the sub-pore scale the impact of the surface structure of a rock was assessed with atomic force microscopy (AFM). As illustrated in Fig. 2., AFM images the topography of a surface mechanically. The surface of the rock is raster scanned by an atomically sharp tip attached to the end of a cantilever. Close to the surface, intermolecular forces acting on the tip lead to a bending of the cantilever, which is monitored by a laser. For the measurements presented, special attention was given to the location at which the rock was scanned, to avoid spots affected by drilling or breakage. The rock surface was scanned with a silicon tip (PPP-NCHAuD from NANOSENSORS™) along a 10 µm x 10 µm area (128 × 128 pixels) using the Quantitative Imaging mode (QI™-mode). In this mode at each pixel a full force distance profile is obtained (i.e. the force between the AFM tip and the surface is monitored as the tip approaches the surface). The rock sample was first saturated with brine and then desaturated with n-decane by flooding (500 µl/min) to mimic the distribution of fluid films and layers at the end of drainage. In addition, test experiments were performed on calcite minerals cleaved in oil and cleaved in brine and then submerged in oil.

The image was analyzed with JPKSPM data processing software (JPK instruments) and then transformed into a 3D image using MATLAB (R2018b). These 3D images were then further processed with Geodict 2015 (Math2Market). A morphological drainage simulation assuming a water-wet contact angle of 30˚ [94] was applied. Avizo 9.0 (a) was used for visualization.

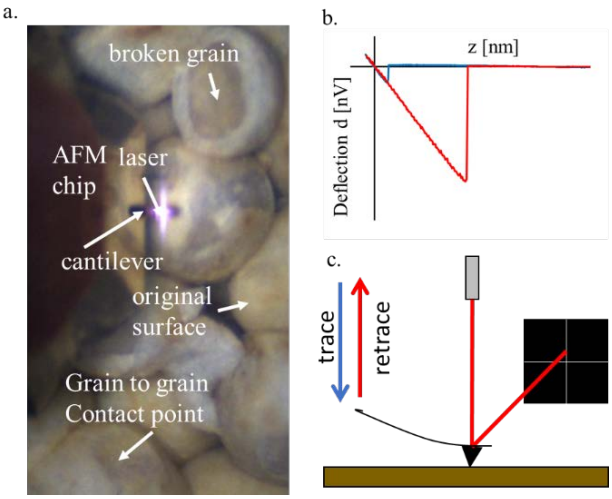

Fig. 2. AFM was used to image the surface of the original rock surface within a pore (a) using QI™-mode, which creates a force distance curve at each pixel (b) by monitoring the deflection of a cantilever with an atomic sharp tip as it approaches and disengages from the surface (c) [71].

3 Results and discussion

3.1 Wettability at the core scale

Fig. 3 shows the core-scale responses obtained from the core-scale steady-state flooding experiment and the Amott spontaneous imbibition test. The results show a difference in wettability depending on the sample initialization.

The samples prepared by flooding appear mixed-wet to water-wet. Following the guidelines to assess wettability from relative permeabilities by Blunt [73], the steady-state experiment initialized by flooding appears with a water permeability end-point of $\boldsymbol{k_{rw}^{max}}$ = 0.2 at the upper limit for a water-wet system, but would not yet be considered mixed-wet. However, with a very low residual oil saturation of $\boldsymbol{S_{res,o}} = 0.06$ and a low water relative permeability at low water saturations (< $\boldsymbol{S_{wi+0.2}}$) of $\boldsymbol{k_{rw}(S_{wi} + 0.2)} = 0.03$, this system fulfils two of three criteria proposed to identify a mixed-wet system and

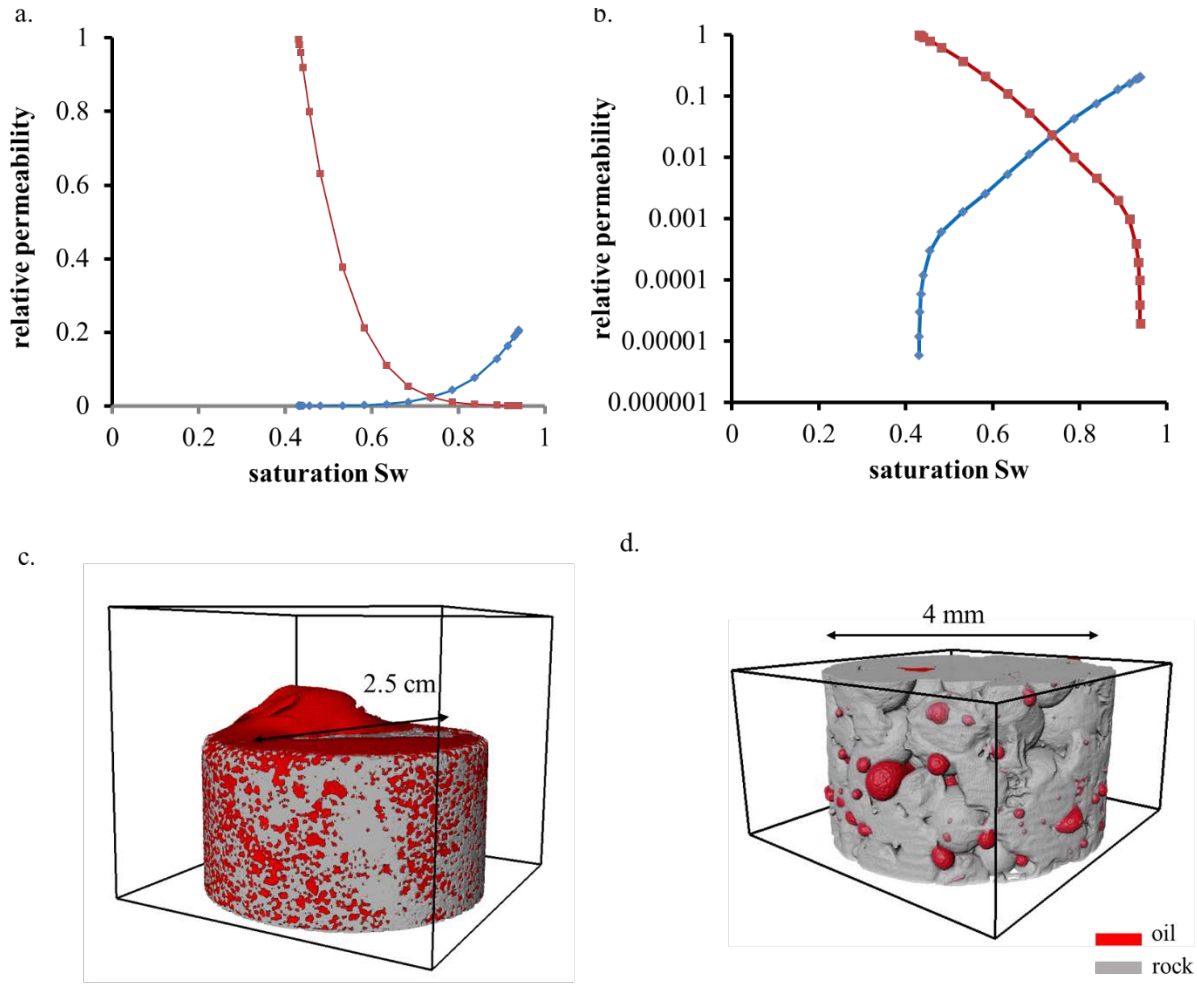

Fig. 3. The core scale steady-state SCAL experiment initialized by flooding shows a relative permeability, here displayed on an arithmetic (a) and semi-logarithmic scale (b), which is typical for a mixed-wet system leaning towards the water-wet side [71]. As the oil droplets (red) emerging from the rock illustrate, the Amott spontaneous imbibition tests show an oil-wet behaviour for the sample initialized by centrifugation (c, imaged using HECTOR) and water-wet behaviour for the sample initialized by flooding (d, imaged using EMCT). [74]

correspondingly is considered mixed-wet leaning to the water-wet side.

The Amott spontaneous imbibition test of the sample initialized by flooding also showed a water-wet response. As illustrated in Fig. 3d the oil droplets emerging while the brine invades the pore space show a water-wet shape. Similar observations for a Ketton rock initialized by flooding have been reported by Alyafei et al. [95].

The sample initialized by centrifugation, however, showed only a little oil production from the pore space (1%) and the oil droplets accumulating at the top of the sample showed an oil-wet structure (Fig. 3c) [77].

The difference between the initialization by flooding and the initialization by centrifugation is the capillary pressure applied during drainage.

Based on the Young-Laplace equation, a higher capillary pressure leads to the invasion of smaller pores by oil compared to a lower capillary pressure. As the rock surface is altered in contact with the crude [22], only the pores invaded by oil are expected to change wettability.

Fig. 4 shows the pore (inlet) diameter distribution of Ketton rock obtained by mercury porosimetry and the estimated pore (inlet) diameter invaded by centrifugation and flooding respectively for the Amott test examples [77]. The pore sizes invaded by centrifugation were estimated based on the rotation speed, interfacial tension and fluid densities assuming an advancing contact angle of 30˚. Based on this calculation pores down to a diameter of 0.3 μm are expected to be filled with oil [77]: this is sufficient to invade some micro-porosity and hence make the solid surfaces oil-wet. As no porous plate was used during flooding the maximum capillary pressure achieved is controlled by the pore structure itself. An exact value cannot be determined. However, the capillary pressure is expected to be at the lower end of the peak pore (inlet) diameter. μCT images obtained with the EMCT scanner after drainage were used for validation. In these images, all the resolved pore sizes showed occupancy with oil. The small amounts of water detected did not show a correlation with the pore diameter. However, it is likely that the micro-porosity in the grains remained water-saturated and water-wet. This is evident in the high initial water saturation of approximately 0.4 in the results shown in Fig. 3. The solid grains are micro-porous – if they are water-filled, they act like a wet sponge and may prevent contact of oil with the surface of the grains even in the larger pores, and hence retaining water-wet characteristics in this case. We will test this directly later in the paper by

measuring water film thicknesses in the corners of the macro-pore space using AFM.

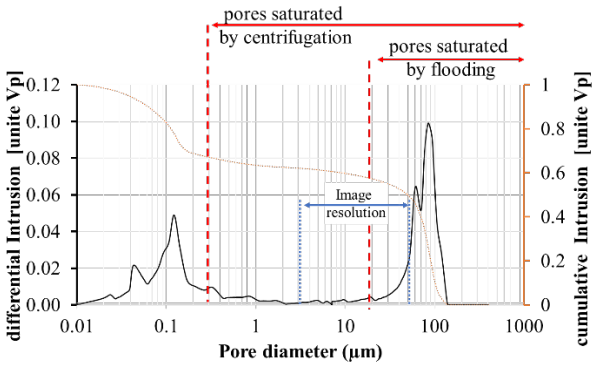

Fig. 4. Pore size distribution of Ketton rock. Based on the oil-saturations obtained from the experiments, initialization by flooding filled pores down to a diameter of 20 µm and centrifugation down to 0.3 µm [77].

Correspondingly, the estimated minimum pore radius accessed during flooding was set at 20 µm at the image resolution boundary (4 voxel lengths) and below the larger peak pore (inlet) diameter (Fig. 4). Smaller scale imaging techniques such as µCT and AFM can give further insights into the core-scale wettability response and will be discussed below in more detail.

3.2 Wettability at the pore scale

The µCT unsteady-state waterflood experiments were used to compare the impact of centrifugation and flooding on sample initialization at the pore-scale.

The images Fig. 5 and Fig. 6 show some examples of the fluid distribution at the pore-scale before and after an unsteady-state waterflood for a sample initialized by flooding (Fig. 5, measured at SLS) and by centrifugation (Fig. 6, measured with Xradia).

Next to the brine phase (white), the oil phase (black) and the rock (light grey) both figures also show the presence of a water-in-oil emulsion. In the sample initialized by flooding the emulsion appears as a third phase (dark grey) [76]. In the sample initialized by centrifugation, the emulsion appears in distinct droplets with a diameter of up to 100 µm. The emulsion forms due to the presence of surface active components in the crude, which are also responsible for the wettability alteration of the system itself. The identification and image processing of this third phase was discussed in detail by Bartels et al. [76].

Furthermore, both figures show the presence of oil films along the grain surface and in the crevices in between after the waterflood. However, for the centrifuged sample, this oil appears continuous, while the oil films in the flooded sample appear discontinuous (comparison Fig. 5 and Fig. 6). This supports the findings observed at the core-scale. The discontinuous oil films observed in the µCT images hint to a mixed-wet sample, while the continuous oil films indicate a predominantly oil-wetting surface. The difference in the emulsion phase can be explained in the same way. As the surface is oil-wet after centrifugation, large water droplets may form and remain stable, while in a mixed-wet system larger droplets are likely to collapse as they get in contact with the preserved water films in a mixed-wet system and only small droplets, (below the image resolution) remain stable.

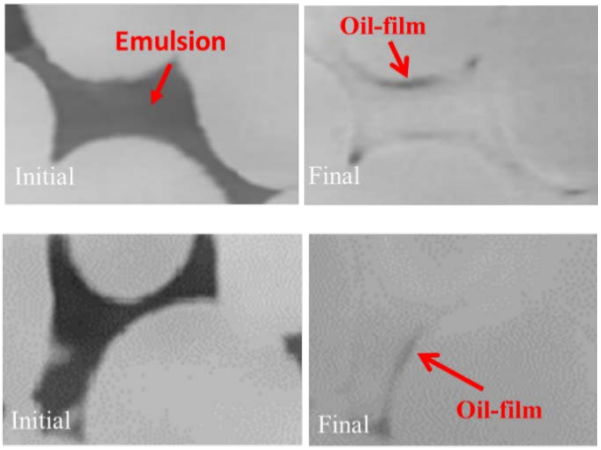

Fig. 5. µCT images obtained before (left) and after the waterflood experiment (right) of a Ketton rock sample (grey) initialized by flooding. Next to the oil (black) and brine (white), the images show the presence of emulsion (dark grey). Furthermore, the images show the presence of discontinuous oil films along the surfaces and in crevices [47, 71]. The images were obtained at the SLS.

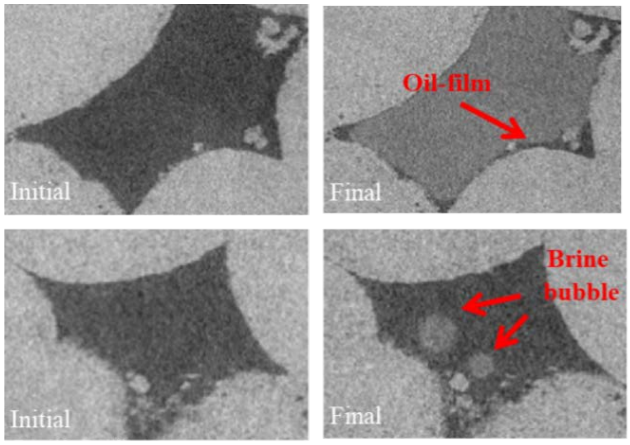

Fig. 6. µCT images obtained before (left) and after the waterflood experiment (right) of a Ketton rock sample initialized by centrifugation. The emulsion phase appears in form of distinct brine droplets. The oil films appear continuous. The images were obtained with Xradia [71].

The images obtained at the end of each waterflood experiment were further used to measure the contact angle distribution displayed in Fig. 6. The contact angle distribution obtained for the Ketton sample indicates a water-wet system with a peak < 90 °. However, compared to the contact angle distribution for the strongly water-wet decane-brine-Ketton rock sample reported by Scanziani et al. [51], this system seems shifted by 30° towards more oil-wet conditions.

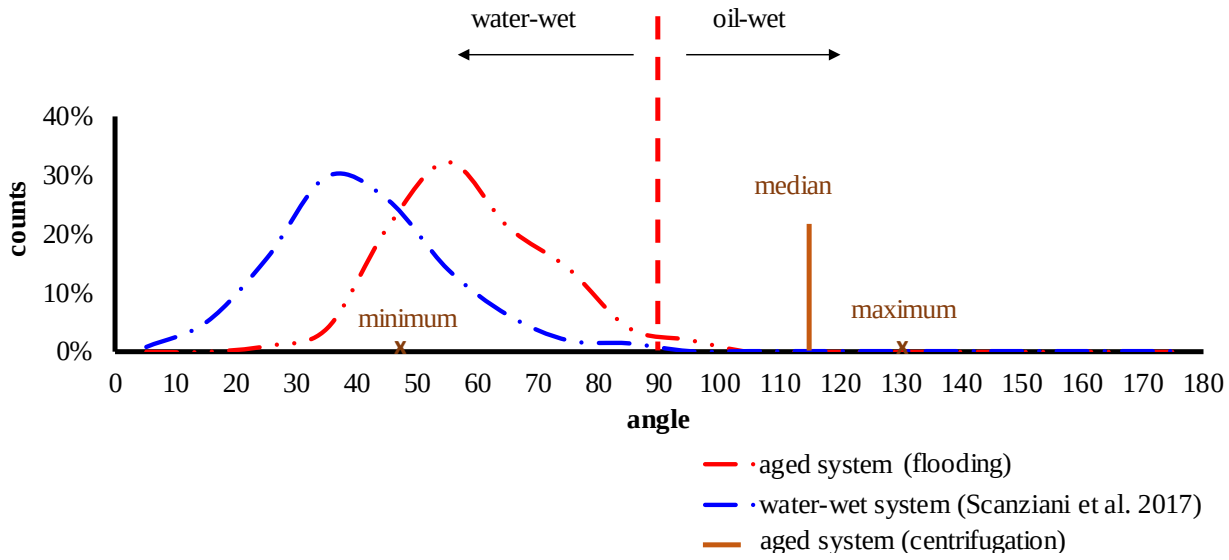

Fig. 7. The contact angle distribution (100 contact angles) for the unsteady-state waterflood µCT experiment with a rock sample initialized by flooding indicates a water-wet state even though more oil-wet than the water-wet reference obtained from Scanziani et al. (2017). Due to the low number of contact angles (21 contact angles) obtained for the unsteady-state waterflood µCT ex-periment performed on a centrifuged sample flooding, solely the median value, the maximum and minimum are plotted [47, 49, 71].

Yet, the contact angle distribution does not show the mixed-wet system observed in the image. The reason might be the patchy small-scale wettability pattern, which leads to pinning of the fluid-fluid interface, when the surface changes from water-wet to oil-wet.

The contact angles detected in the sample initialized by centrifugation varied from 50 ˚ to 130˚, with a median value of 115˚ (Fig. 7). Only 21 contact angles could be obtained for this sample. The reason was that the oil remained predominantly in the poorly resolved pore throats, which are less suitable for contact angle measurements. For the same reason, the contact angles obtained may be more affected by measurement errors, which needs to be considered for the following interpretation: The low values of 50˚ might be a sign of a mixed-wettability pattern. However, as the oil-phase in this sample is continuous, the pinning of the fluid-fluid interface is less pronounced.

The sample initialization of the two cores investigated were subject to different capillary pressures applied during the drainage process and aging time. However, the impact of aging time was assumed to be minor for the following reasons. First, the core-scale studies indicate that the wettability alteration of Ketton rock appears already after 24h. Second, previous studies indicated that the water-wet appearance of Ketton rock is preserved for even longer aging periods [95]. Third, oil layers, present in the flooded sample, show that wettability alteration happened where the oil was in contact with the surface. The oil layer, however, was discontinuous, which might have been caused by sub-resolution surface features, which can be investigated with AFM.

3.3 Wettability at the sub-pore scale

AFM was utilized to investigate the water films and layers present within the Ketton rock sample initialized by flooding.

The water-decane interface and the height of the rock surface were obtained from the force distance curves collected for all of the 128 × 128 pixels along the 10 µm × 10 µm area. Fig. 8 shows examples for such force distance curves obtained from measurements on calcite surfaces prepared with and without water.

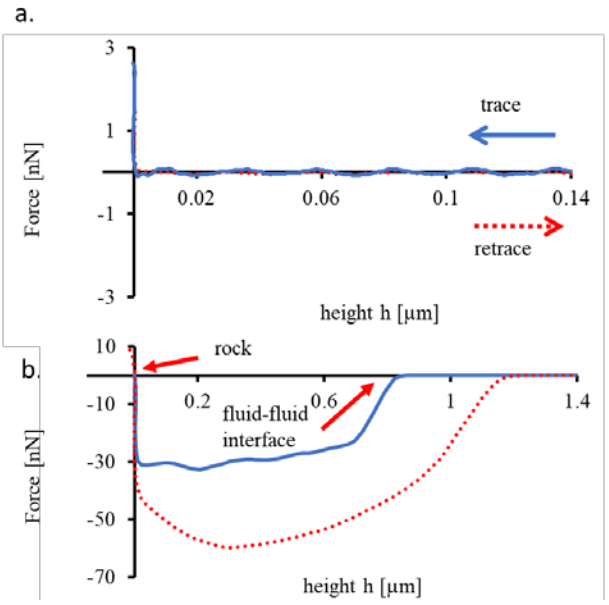

Fig. 8. Representative force distance curves obtained from a calcite surface without (a) and with the presence of a water film (b). As the tip passes through the brine-decane interface the cantilever is bending towards the surface, which is recorded as a negative force. Once the cantilever reaches the rock surface it gets bent in the opposite direction [71].

As the tip is water-wet, the cantilever bends towards the surface when it passes through the fluid-fluid interface during the approach, which is displayed in form of a negative force. The height of the rock surface is obtained

from the bending of the tip in the opposite direction recorded as a positive force on the cantilever.

In the resulting image shown in Fig. 9, 60% of the surface was covered with brine. Only 40% of the surface were directly in contact with decane.

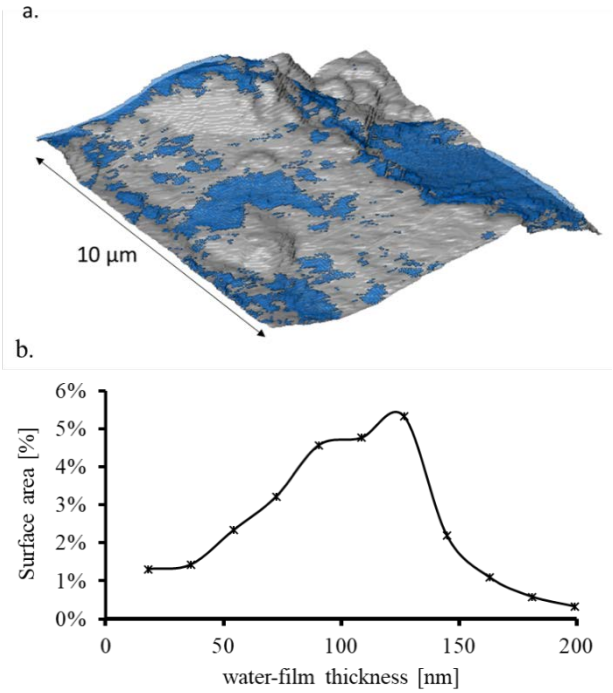

Fig.10. a Water film (blue) on top of a rock surface (grey) measured in decane. The water layer shows a film thickness ranging between 0 nm and 200 nm with a peak film thickness of 125nm (b) [71].

The 3D measurement of the wetting film also allows to quantify fluid film thickness. Fig.9b shows that the film thickness ranges between 0 nm and 200 nm with a peak film thickness of 125 nm.

Furthermore, the rock surface obtained was used to simulate the coverage of the rock for different capillary pressures applied using a morphological drainage simulation. The algorithm fits spheres of different radii, representing different capillary pressures, onto the surface to model the drainage process as it is applied prior to the wettability alteration in a rock.

The result is shown in Fig. 10. Fig. 10d shows the surface area coverage as a function of sphere diameter. The higher the diameter – and the lower the corresponding capillary pressure – the larger the surface area covered with brine. 50% of the surface was covered with water for a sphere diameter of 7 µm. For sphere diameters below 1.5 µm only 1.5% of the surface remained in contact with the aqueous phase. These results are in line with the detected water films.

These findings show that surface roughness of a rock can facilitate the formation of water-layers. Different capillary pressures applied on the rock during drainage result in different water coverage of the rock surface. Based on the assumption that wettability alteration occurs predominantly when the surface is in direct contact with the oil, the difference in coverage would result in a sub-pore-scale wettability pattern as indicated in section 3.2 and explain the different wettability responses observed at the core-scale.

4 Conclusions

In this study we assessed the wettability across the length scales using similar oil-brine-rock system, including AFM at the sub-pore scale, µCT imaging and *in situ* contact angle distributions at the pore-scale combined with Amott spontaneous imbibition tests and steady-state relative permeability measurements at the core-scale, demonstrating that upscaling is possible.

For this crude oil-brine-rock system, surface roughness and the capillary pressure applied during initialization were found to control the larger scale wettability response after aging.

AFM studies showed the formation of water films along the rock surface preventing a direct contact of the oil and the rock which lead to a patchy sub-pore scale

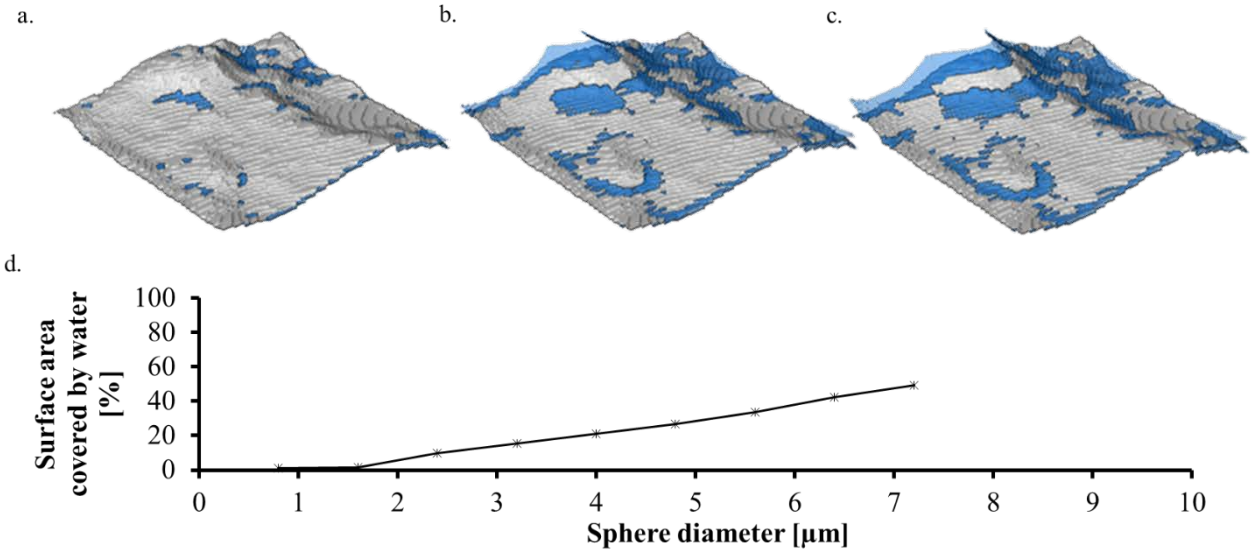

Fig. 9. Water films (blue) on top of a rock surface (grey) obtained from a drainage simulation based on sphere fitting (a: sphere diameter = 1.6 µm, b: sphere diameter = 5.6 µm, c: sphere diameter = 6 µm). d shows the percentage of surface area covered with brine as a function of sphere diameter [71].

wettability pattern after aging. This small-scale wettability pattern leads to a water-wet contact angle distribution at the pore-scale, while some surface show discontinuous oil layers and a mixed-wet core-scale response leaning towards the water-wet side.

Furthermore, nano-scale simulations showed that the higher the capillary pressure, the larger the oil-rock contact area. Once the oil film becomes continuous the core scale response for the same system appears oil-wet at the pore- and core-scale.

This study demonstrates that for predictions of the core-scale wettability response, the nano-scale surface structure of the rock needs to be considered.

Acknowledgments

We would like to acknowledge the staff of UGCT, Ghent, Belgium for support for the spontaneous imbibition experiment and the Paul Scherrer Institute, Villigen, Switzerland for the provision of synchrotron radiation beamtime at TOMCAT beamline of the SLS and for assistance during the session. Furthermore, we would like to thank Anne Bonnin, Christian Hinz, Arne Jacob, Christian Wagner, Steven Henkel and Frieder Enzmann for support during the beamline experiments. We would like to acknowledge Alex Schwing and Rob Neiteler for the design of the setup and instrumentation, Fons Marcelis for sample preparation, Holger Ott, Ryan Armstrong and James McClure, Alex Winkel, Hayley Meek, Matthew Leivers, Tannaz Pak, the Shell Digital Rock team at Imperial and the team from Math2Market for helpful discussions. We gratefully acknowledge Shell Global Solutions International B.V. for their permission to publish this work.

References

1. R. J. S. Brown and I. Fatt, "Measurements Of Fractional Wettability Of Oil Fields' Rocks By The Nuclear Magnetic Relaxation Method," presented at the Fall Meeting of the Petroleum Branch of AIME, Los Angeles, California, 1956.

2. E. C. Donaldson and W. Alam, "CHAPTER 1 - Wettability," in *Wettability*: Gulf Publishing Company, 2008, pp. 1-55.

3. R. A. Salathiel, "Oil Recovery by Surface Film Drainage In Mixed-Wettability Rocks," *Journal of Petroleum Technology*, vol. 25, no. 10, pp. 1216-1224, 1973, Art. no. SPE-4104-PA.

4. W. Anderson, "Wettability Literature Survey- Part 1: Rock/Oil/Brine Interactions and the Effects of Core Handling on Wettability," *Journal of Petroleum Technology*, vol. 38, no. 10, pp. 1125-1144, 1986, Art. no. SPE-13932-PA.

5. W. Abdallah *et al.*, "Fundamentals of wettability," *Schlumberger Oilfield Review*, vol. 19/2, pp. 44-61, 2007.

6. E. C. Donaldson and W. Alam, "CHAPTER 3 - Wettability and Production," in *Wettability*: Gulf Publishing Company, 2008, pp. 121-172.

7. W. Anderson, "Wettability Literature Survey- Part 4: Effects of Wettability on Capillary Pressure," *Journal of Petroleum Technology*, vol. 39, no. 10, pp. 1,283 - 1,300, 1987, Art. no. SPE-15271-PA.

8. W. Anderson, "Wettability Literature Survey Part 5: The Effects of Wettability on Relative Permeability," *Journal of Petroleum Technology*, vol. 39, no. 11, pp. 1453-1468, 1987, Art. no. SPE-16323-PA.

9. T. Hassenkam, L. L. Skovbjerg, and S. L. S. Stipp, "Probing the intrinsically oil-wet surfaces of pores in North Sea chalk at subpore resolution," *Proceedings of the National Academy of Sciences*, vol. 106, no. 15, pp. 6071-6076, 2009.

10. T. Hassenkam *et al.*, "Could Atomic-Force Microscopy Force Mapping Be a Fast Alternative to Core-Plug Tests for Optimizing Injection-Water Salinity for Enhanced Oil Recovery in Sandstone?," *SPE Journal*, vol. 21, no. 03, pp. 720 - 729, 2015, Art. no. SPE-169136-PA.

11. J. Matthiesen *et al.*, "How Naturally Adsorbed Material on Minerals Affects Low Salinity Enhanced Oil Recovery," *Energy & Fuels*, vol. 28, no. 8, pp. 4849-4858, 2014.

12. N. R. Morrow, "The Effects of Surface Roughness On Contact: Angle With Special Reference to Petroleum Recovery," *Journal of Canadian Petroleum Technology*, vol. 14, no. 04, pp. 0021-9487, 1975.

13. M. Andrew, B. Bijeljic, and M. J. Blunt, "Pore-scale contact angle measurements at reservoir conditions using X-ray microtomography," *Advances in Water Resources*, vol. 68, pp. 24-31, 2014.

14. A. L. Herring, E. J. Harper, L. Andersson, A. Sheppard, B. K. Bay, and D. Wildenschild, "Effect of fluid topology on residual nonwetting phase trapping: Implications for geologic CO2 sequestration," *ADV WATER RESOUR*, vol. 62, pp. 47-58, 2013.

15. A. L. Herring, A. Sheppard, L. Andersson, and D. Wildenschild, "Impact of wettability alteration on 3D nonwetting phase trapping and transport," *International Journal of Greenhouse Gas Control*, vol. 46, pp. 175-186, 2016.

16. R. T. Armstrong, M. L. Porter, and D. Wildenschild, "Linking pore-scale interfacial curvature to column-scale capillary pressure," *Advances in Water Resources*, vol. 46, pp. 55-62, 2012.

17. T. Bultreys *et al.*, "Validation of model predictions of pore-scale fluid distributions during two-phase flow," *Physical Review E,* vol. 97, no. 5, p. 053104, 2018.

18. S. Berg *et al.*, "Connected pathway relative permeability from pore-scale imaging of imbibition," *Advances in Water Resources,* vol. 90, pp. 24-35, 2016.

19. F. C. Benner, W. W. Riches, and F. E. Bartell, "Nature and Importance of Surface Forces in Production of Petroleum," presented at the Drilling and Production Practice, Amarillo, Texas, 1938.

20. K. Kumar, E. Dao, and K. Mohanty, "Atomic force microscopy study of wettability alteration," presented at the SPE International Symposium on Oilfield Chemistry, The Woodlands, Texas 2005.

21. M. A. Fernø, M. Torsvik, S. Haugland, and A. Graue, "Dynamic Laboratory Wettability Alteration," *Energy & Fuels,* vol. 24, no. 7, pp. 3950-3958, 2010.

22. J. S. Buckley, "Effective wettability of minerals exposed to crude oil," *Current Opinion in Colloid & Interface Science,* vol. 6, no. 3, pp. 191-196, 2001.

23. M. S. Akhlaq, D. Kessel, and W. Dornow, "Separation and Chemical Characterization of Wetting Crude Oil Compounds," *Journal of Colloid and Interface Science,* vol. 180, no. 2, pp. 309-314, 1996.

24. M. White, K. Pierce, and T. Acharya, "A Review of Wax-Formation/Mitigation Technologies in the Petroleum Industry," *SPE Production & Operations,* vol. 33, no. 03, pp. 476 - 485, 2017, Art. no. SPE-189447-PA.

25. T. Fan, J. Wang, and J. S. Buckley, "Evaluating Crude Oils by SARA Analysis," presented at the SPE/DOE Improved Oil Recovery Symposium, Tulsa, Oklahoma, 2002.

26. B. Derjaguin and L. Landau, "Theory of the stability of strongly charged lyophobic sols and of the adhesion of strongly charged particles in solutions of electrolytes," *Acta Physico Chimica URSS,* vol. 14, no. 633, 1941.

27. J. T. G. Overbeek and E. Verwey, *Theory of the Stability of Lyophobic Colloids: The interaction of Sol Particles Having an Electric Double Layer*. New York-Amsterdam: Elsevier Publishing Company., 1948.

28. J. N. Israelachvili, "17 - Adhesion and Wetting Phenomena," in *Intermolecular and Surface Forces (Third Edition)*San Diego: Academic Press, 2011, pp. 415-467.

29. G. J. Hirasaki, "Wettability: Fundamentals and Surface Forces," *SPE Formation Evaluation,* vol. 6, no. 02, pp. 217 - 226, 1991, Art. no. SPE-17367-PA.

30. C. Drummond and J. Israelachvili, "Fundamental studies of crude oil–surface water interactions and its relationship to reservoir wettability," *Journal of Petroleum Science and Engineering,* vol. 45, no. 1-2, pp. 61-81, 2004.

31. W. B. Bartels, H. Mahani, S. Berg, and S. M. Hassanizadeh, "Literature review of low salinity waterflooding from a length and time scale perspective," *Fuel,* vol. 236, pp. 338-353, 2019.

32. J. S. Buckley, Y. Liu, X. Xie, and N. R. Morrow, "Asphaltenes and Crude Oil Wetting - The Effect of Oil Composition," *SPE Journal,* vol. 2, no. 02, pp. 107-119, 1997, Art. no. SPE-35366-PA.

33. P. Purswani, M. S. Tawfik, and Z. T. Karpyn, "Factors and Mechanisms Governing Wettability Alteration by Chemically Tuned Waterflooding: A Review," *Energy & Fuels,* vol. 31, no. 8, pp. 7734-7745, 2017.

34. A. Mennella, N. R. Morrow, and X. Xie, "Application of the dynamic Wilhelmy plate to identification of slippage at a liquid-liquid-solid three-phase line of contact," *Journal of Petroleum Science and Engineering,* vol. 13, no. 3, pp. 179-192, 1995.

35. Y. Deng, L. Xu, H. Lu, H. Wang, and Y. Shi, Direct measurement of the contact angle of water droplet on quartz in a reservoir rock with atomic force microscopy," *Chemical Engineering Science,* vol. 177, pp. 445-454, 2018.

36. R. Giro, P. W. Bryant, M. Engel, R. F. Neumann, and M. B. Steiner, "Adsorption energy as a metric for wettability at the nanoscale," *Scientific Reports,* vol. 7, p. 46317, 2017.

37. L. E. Treiber and W. W. Owens, "A Laboratory Evaluation of the Wettability of Fifty Oil-Producing Reservoirs," *SPE Journal,* vol. 12, no. 06, pp. 531 - 540, 1972, Art. no. SPE-3526-PA.

38. R. O. Leach, O. R. Wagner, H. W. Wood, and C. F. Harpke, "A Laboratory and Field Study of Wettability Adjustment in Water Flooding," *Journal of Petroleum Technology,* vol. 14, no. 02, pp. 206-212, 1962, Art. no. SPE-119-PA.

39. F. G. McCaffery and N. Mungan, "Contact Angle And Interfacial Tension Studies of Some Hydrocarbon-Water-Solid Systems," *Journal of Canadian Petroleum Technology,* vol. 9, no. 03, pp. 185-196, 1970.

40. O. S. Hjelmeland and L. E. Larrondo, "Experimental Investigation of the Effects of Temperature, Pressure, and Crude Oil Composition on Interfacial Properties," *SPE Reservoir Engineering*, vol. 1, no. 04, pp. 321-328, 1986.

41. A. W. Neumann and R. J. Good, "Techniques of Measuring Contact Angles," in *Surface and Colloid Science: Volume 11: Experimental Methods*, R. J. Good and R. R. Stromberg, Eds. Boston, MA: Springer US, 1979, pp. 31-91.

42. D. Broseta, N. Tonnet, and V. Shah, "Are rocks still water-wet in the presence of dense CO2 or H2S?," *Geofluids*, vol. 12, no. 4, pp. 280-294, 2012.

43. R. N. Wenzel, "RESISTANCE OF SOLID SURFACES TO WETTING BY WATER," *Industrial & Engineering Chemistry*, vol. 28, no. 8, pp. 988-994, 1936.

44. A. Fogden, "Effect of Water Salinity and pH on the Wettability of a Model Substrate," *Energy & Fuels*, vol. 25, no. 11, pp. 5113-5125, 2011.

45. E. E. Santiso, C. Herdes, and E. A. Müller, "On the Calculation of Solid-Fluid Contact Angles from Molecular Dynamics," *Entropy*, vol. 15, no. 9, pp. 3734-3745, 2013.

46. A. R. Kovscek, H. Wong, and C. J. Radke, "A pore-level scenario for the development of mixed wettability in oil reservoirs," *AIChE Journal*, vol. 39, no. 6, pp. 1072-1085, 1993.

47. D. Quéré, "Wetting and Roughness," *Annual Review of Materials Research*, vol. 38, no. 1, pp. 71-99, 2008.

48. S. Herminghaus, "Roughness-induced non-wetting," *Europhysics Letters*, vol. 52, no. 2, pp. 165-170, 2000.

49. M. Rücker *et al.*, "The Effect of Mixed Wettability on Pore-Scale Flow Regimes Based on a Flooding Experiment in Ketton Limestone," *Geophysical Research Letters*, vol. 46, no. 6, pp. 3225-3234, 2019.

50. J. S. Buckley, C. Bousseau, and Y. Liu, "Wetting Alteration by Brine and Crude Oil: From Contact Angles to Cores," *SPE Journal*, vol. 1, no. 03, pp. 341-350, 1996, Art. no. SPE-30765-PA.

51. A. Scanziani, K. Singh, M. J. Blunt, and A. Guadagnini, "Automatic method for estimation of in situ effective contact angle from X-ray micro tomography images of two-phase flow in porous media," *Journal of Colloid and Interface Science*, vol. 496, pp. 51-59, 2017.

52. A. AlRatrout, A. Q. Raeini, B. Bijeljic, and M. J. Blunt, "Automatic measurement of contact angle in pore-space images," *Advances in Water Resources*, vol. 109, pp. 158-169, 2017.

53. A. M. Alhammadi, A. AlRatrout, K. Singh, B. Bijeljic, and M. J. Blunt, "In situ characterization of mixed-wettability in a reservoir rock at subsurface conditions," *Scientific Reports*, vol. 7, no. 1, p. 10753, 2017.

54. S. Iglauer, M. Fernø, P. Shearing, and M. Blunt, "Comparison of residual oil cluster size distribution, morphology and saturation in oil-wet and water-wet sandstone," *Journal of colloid and interface science*, vol. 375, no. 1, pp. 187-192, 2012.

55. R. I. Al-Raoush, "Impact of Wettability on Pore-Scale Characteristics of Residual Nonaqueous Phase Liquids," *Environmental Science & Technology*, vol. 43, no. 13, pp. 4796-4801, 2009.

56. K. Singh, B. Bijeljic, and M. J. Blunt, "Imaging of oil layers, curvature and contact angle in a mixed-wet and a water-wet carbonate rock," *Water Resources Research*, vol. 52, no. 3, pp. 1716-1728, 2016.

57. Q. Lin, B. Bijeljic, S. Berg, R. Pini, M. J. Blunt, and S. Krevor, "Minimal surfaces in porous media: Pore-scale imaging of multiphase flow in an altered-wettability Bentheimer sandstone," *Physical Review E*, vol. 99, no. 6, p. 063105, 2019.

58. P. Lehmann *et al.*, "Impact of geometrical properties on permeability and fluid phase distribution in porous media," *Advances in Water Resources*, vol. 31, no. 9, pp. 1188-1204, 2008.

59. V. Joekar-Niasar, S. M. Hassanizadeh, and A. Leijnse, "Insights into the Relationships Among Capillary Pressure, Saturation, Interfacial Area and Relative Permeability Using Pore-Network Modeling," *Transport in Porous Media*, journal article vol. 74, no. 2, pp. 201-219, 2008.

60. H. J. Vogel, U. Weller, and S. Schlüter, "Quantification of soil structure based on Minkowski functions," *Computers & Geosciences*, vol. 36, no. 10, pp. 1236-1245, 2010.

61. S. Schlüter *et al.*, "Pore-scale displacement mechanisms as a source of hysteresis for two-phase flow in porous media," *Water Resources Research*, vol. 52, no. 3, pp. 2194-2205, 2016.

62. R. T. Armstrong *et al.*, "Porous Media Characterization Using Minkowski Functionals: Theories, Applications and Future Directions," *Transport in Porous Media*, journal article 2018.

63. A. L. Herring, J. Middleton, R. Walsh, A. Kingston, and A. Sheppard, "Flow rate impacts on capillary pressure and interface curvature of connected and disconnected fluid phases during multiphase flow in sandstone," *Advances in Water Resources*, vol. 107, pp. 460-469, 2017.

64. S. Zou, R. T. Armstrong, J.-Y. Arns, C. H. Arns, and F. Hussain, "Experimental and Theoretical Evidence for Increased Ganglion Dynamics During Fractional Flow in Mixed-Wet Porous Media," *Water Resources Research*, vol. 54, no. 5, pp. 3277-3289, 2018.

65. Q. Lin, B. Bijeljic, R. Pini, M. J. Blunt, and S. Krevor, "Imaging and Measurement of Pore-Scale Interfacial Curvature to Determine Capillary Pressure Simultaneously With Relative Permeability," *Water Resources Research*, vol. 54, no. 9, pp. 7046-7060, 2018.

66. E. C. Donaldson, R. D. Thomas, and P. B. Lorenz, "Wettability Determination and Its Effect on Recovery Efficiency," *SPE Journal*, vol. 9, no. 01, pp. 13 - 20, 1969.

67. E. Amott, "Observations Relating to the Wettability of Porous Rock," *Petroleum Transactions, AIME*, vol. 216, pp. 156-162, 1959, Art. no. SPE-1167-G.

68. C. C. Mattax and J. Kyte, "Imbibition oil recovery from fractured, water-drive reservoir," *SPE Journal*, vol. 2, no. 02, pp. 177-184, 1962, Art. no. SPE-187-PA.

69. S. Ma, N. Morrow, and X. Zhang, "Generalized scaling of spontaneous imbibition data for strongly water-wet systems," presented at the Technical Meeting/Petroleum Conference of The South Saskatchewan Section, Regina, Canada, 1995.

70. K. S. Schmid and S. Geiger, "Universal scaling of spontaneous imbibition for arbitrary petrophysical properties: Water-wet and mixed-wet states and Handy's conjecture," *Journal of Petroleum Science and Engineering*, vol. 101, pp. 44-61, 2013.

71. M. C. Leverett, "Capillary Behavior in Porous Solids," *Transactions of the AIME*, vol. 142, no. 01, pp. 152-169, 1941.

72. S. Zou and R. Armstrong, "Multiphase Flow Under Heterogeneous Wettability Conditions Studied by Special Core Analysis and Pore-Scale Imaging," *SPE Journal*, vol. 24, no. 03, pp. 1234-1247, 2019.

73. M. J. Blunt, *Multiphase flow in permeable media: a pore-scale perspective*. Cambridge, UK: Cambridge University Press, 2017.

74. M. Rücker, "Wettability and wettability alteration at the pore- and nano- scales," PhD Thesis, Imperial College London, 2018.

75. W. Bartels, "Pore scale processes in mixed-wet systems with application to low salinity waterflooding," PhD PhD Thesis, UU Dept. of Earth Sciences, 2018.

76. W. B. Bartels *et al.*, "Fast X-Ray Micro-CT Study of the Impact of Brine Salinity on the Pore-Scale Fluid Distribution During Waterflooding," *Petrophysics*, vol. 58, no. 01, pp. 36-47, 2017.

77. W. Bartels *et al.*, "Pore-scale displacement during fast imaging of spontaneous imbibition " presented at the International Symposium of the Society of Core Analysts, Vienna, Austria, 2017.

78. H. Mahani, A. L. Keya, S. Berg, W.-B. Bartels, R. Nasralla, and W. R. Rossen, "Insights into the Mechanism of Wettability Alteration by Low-Salinity Flooding (LSF) in Carbonates," *Energy & Fuels*, vol. 29, no. 3, pp. 1352-1367, 2015.

79. E. Flügel, *Microfacies of carbonate rocks: analysis, interpretation and application*. Springer Science & Business Media, 2013.

80. K. Singh *et al.*, "Dynamics of snap-off and pore-filling events during two-phase fluid flow in permeable media," *Scientific Reports*, vol. 7, p. 5192, 2017.

81. M. Andrew, H. Menke, M. J. Blunt, and B. Bijeljic, "The Imaging of Dynamic Multiphase Fluid Flow Using Synchrotron-Based X-ray Microtomography at Reservoir Conditions," *Transport In Porous Media*, journal article vol. 110, no. 1, pp. 1-24, 2015.

82. M. Andrew, "Reservoir-Condition Pore-Scale Imaging of Multiphase Flow," PhD PhD Thesis, Earth Science and Engineering, Imperial College London, London, 2015.

83. J. Kokkedee, W. Boom, A. Frens, and J. Maas, "Improved special core analysis: scope for a reduced residual oil saturation," presented at the Society of core analysis conference paper, Montpellier, France, 1996.

84. S. Berg, A. W. Cense, J. P. Hofman, and R. M. M. Smits, "Two-Phase Flow in Porous Media with Slip Boundary Condition," *Transport in Porous Media*, journal article vol. 74, no. 3, pp. 275-292, 2008.

85. C. McPhee, J. Reed, and I. Zubizarreta, *Core Analysis: A Best Practice Guide*. Amsterdam, The Netherlands: Elsevier, 2015.

86. L. Dake, *Fundamentals of Reservoir Engineering., 1978*. Elsevier, New York, 1983.

87. B. Masschaele *et al.*, "HECTOR: A 240kV micro-CT setup optimized for research," *Journal of Physics: Conference Series,* vol. 463, p. 012012, 2013.

88. T. Bultreys, W. De Boever, and V. Cnudde, "Imaging and image-based fluid transport modeling at the pore scale in geological materials: A practical introduction to the current state-of-the-art," *Earth-Science Reviews,* vol. 155, pp. 93-128, 2016.

89. Q. Lin *et al.*, "A New Waterflood Initialization Protocol With Wettability Alteration for Pore-Scale Multiphase Flow Experiments," *Petrophysics,* vol. 60, no. 02, pp. 264-272, 2019.

90. M. Rücker *et al.*, "A time-resolved synchrotron X-ray micro-tomography dataset of a waterflood in an altered mixed-wet Ketton limestone," ed: Digital Rocks Portal, 2019.

91. D. Paganin, S. Mayo, T. E. Gureyev, P. R. Miller, and S. W. Wilkins, "Simultaneous phase and amplitude extraction from a single defocused image of a homogeneous object," *Journal of Microscopy,* vol. 206, no. 1, pp. 33-40, 2002.

92. I. Arganda-Carreras *et al.*, "Trainable Weka Segmentation: a machine learning tool for microscopy pixel classification," *Bioinformatics,* vol. 33, no. 15, pp. 2424-2426, 2017.

93. J. Schindelin *et al.*, "Fiji: an open-source platform for biological-image analysis," *Nature Methods*, Perspective vol. 9, p. 676, 2012.

94. M. Hilpert and C. T. Miller, "Pore-morphology-based simulation of drainage in totally wetting porous media," *Advances in Water Resources,* vol. 24, no. 3, pp. 243-255, 2001.

95. N. Alyafei and M. J. Blunt, "The effect of wettability on capillary trapping in carbonates," *Advances in Water Resources*, vol. 90, no. Supplement C, pp. 36-50, 2016.